




Antisense oligonucleotides restore excitability, GABA signalling and sodium current density in a Dravet syndrome model

Yukun Yuan,¹ Luis Lopez-Santiago,¹ Nicholas Denomme,¹ Chunling Chen,¹ Heather A. O'Malley,¹ Samantha L. Hodges,¹ Sophina Ji,² Zhou Han,² Anne Christiansen² and  Lori L. Isom¹

Dravet syndrome is an intractable developmental and epileptic encephalopathy caused by *de novo* variants in *SCN1A* resulting in haploinsufficiency of the voltage-gated sodium channel $\text{Na}_v1.1$. We showed previously that administration of the antisense oligonucleotide STK-001, also called ASO-22, generated using targeted augmentation of nuclear gene output technology to prevent inclusion of the nonsense-mediated decay, or poison, exon 20N in human *SCN1A*, increased productive *Scn1a* transcript and $\text{Na}_v1.1$ expression and reduced the incidence of electrographic seizures and sudden unexpected death in epilepsy in a mouse model of Dravet syndrome. Here, we investigated the mechanism of action of ASO-84, a surrogate for ASO-22 that also targets splicing of *SCN1A* exon 20N, in *Scn1a*^{+/-} Dravet syndrome mouse brain.

Scn1a^{+/-} Dravet syndrome and wild-type mice received a single intracerebroventricular injection of antisense oligonucleotide or vehicle at postnatal Day 2. We examined the electrophysiological properties of cortical pyramidal neurons and parvalbumin-positive fast-spiking interneurons in brain slices at postnatal Days 21–25 and measured sodium currents in parvalbumin-positive interneurons acutely dissociated from postnatal Day 21–25 brain slices. We show that, in untreated Dravet syndrome mice, intrinsic cortical pyramidal neuron excitability was unchanged while cortical parvalbumin-positive interneurons showed biphasic excitability with initial hyperexcitability followed by hypoexcitability and depolarization block. Dravet syndrome parvalbumin-positive interneuron sodium current density was decreased compared to wild-type. GABAergic signalling to cortical pyramidal neurons was reduced in Dravet syndrome mice, suggesting decreased GABA release from interneurons. ASO-84 treatment restored action potential firing, sodium current density and GABAergic signalling in Dravet syndrome parvalbumin-positive interneurons. Our work suggests that interneuron excitability is selectively affected by ASO-84.

This new work provides critical insights into the mechanism of action of this antisense oligonucleotide and supports the potential of antisense oligonucleotide-mediated upregulation of $\text{Na}_v1.1$ as a successful strategy to treat Dravet syndrome.

¹ Department of Pharmacology, University of Michigan, Ann Arbor, MI 48109, USA

² Stoke Therapeutics, Inc., Bedford, MA 01730, USA

Correspondence to: Lori L. Isom, PhD

Department of Pharmacology, 2301 E MSRB III, Ann Arbor, MI 48109-5632, USA

E-mail: lisom@umich.edu

Keywords: sodium channel; epilepsy; antisense oligonucleotide; therapeutics

Introduction

Dravet syndrome is a devastating form of developmental and epileptic encephalopathy (DEE). In >80% of cases, Dravet syndrome is caused by *de novo* variants in SCN1A, encoding the voltage-gated sodium channel (VGSC) α subunit Na_v1.1, resulting in haploinsufficiency (DEE6, OMIM 607208).^{1,2} Dravet syndrome patients have severe epilepsy, intellectual disability, developmental delays, movement and balance issues, language and speech disturbances, growth defects, sleep abnormalities, chronic infections, disruptions of the autonomic nervous system and mood disorders.^{3–7} While all patients with epilepsy are at risk for sudden unexpected death in epilepsy (SUDEP), patients with Dravet syndrome have an extraordinarily high risk, of up to 20%.⁸ The prevalence of Dravet syndrome in the US population has been estimated to be as high as 1:15 700, a population of ~20 000 individuals.⁹ While recently developed small molecule anticonvulsant therapies^{10,11} provide partial seizure management for some Dravet syndrome patients, there remains a significant, unmet need for novel approaches to directly target the root cause of the disease in brain, SCN1A haploinsufficiency.⁶

Targeted augmentation of nuclear gene output (TANGO) was developed to increase protein expression in diseases of haploinsufficiency using antisense oligonucleotide (ASO) technology.¹² TANGO targets naturally occurring, alternative splicing events to reduce non-productive mRNA and increase productive mRNA and protein of the target gene by upregulating the wild-type allele.^{12,13} This approach has provided a unique opportunity to develop novel therapeutics to treat Dravet syndrome. We showed previously that a single, intracerebroventricular (ICV) dose of STK-001, also called ASO-22, generated using TANGO technology to prevent inclusion of a nonsense-mediated decay (NMD), or poison, exon in human SCN1A, exon 20N, increased productive *Scn1a* transcript and Na_v1.1 expression and reduced the incidence of electrographic seizures and SUDEP in a mouse model of Dravet syndrome.¹³ Interestingly, *de novo* variants in exon 20N increase its inclusion, resulting in haploinsufficiency and Dravet syndrome pathology in patients and in a mouse model.^{14,15} Here, we investigated the mechanism of an ASO that also targets SCN1A exon 20N, ASO-84, in Dravet syndrome mouse brain. We tested the effects of a single ICV injection of ASO-84 at postnatal Day (P)2 on the subsequent electrophysiological properties of cortical pyramidal and parvalbumin-positive (PV+) fast-spiking interneurons in *Scn1a*^{+/-} Dravet syndrome and *Scn1a*^{+/+} wild-type (WT) littermate mice at P21–25. We show that, in untreated Dravet syndrome mice, intrinsic action potential (AP) firing properties of cortical pyramidal neurons were unchanged compared to controls. In contrast, AP firing properties showed depolarization block and sodium current density was reduced in Dravet syndrome PV+ interneurons. The frequency, but not amplitude, of inhibitory post-synaptic currents (IPSCs) recorded in Dravet syndrome cortical pyramidal neurons was also reduced, suggesting reduced GABA release from interneurons. Single-dose ASO-84 administration restored excitability and sodium current density in PV + Dravet syndrome interneurons as well as restored GABAergic signalling to cortical pyramidal neurons. This new work provides key mechanisms for further development of precision medicine approaches to treat patients with Dravet syndrome and related DEEs.

Materials and methods

Animals

Mouse studies were performed in compliance with protocols approved by the University of Michigan Institutional Animal Care and

Use Committee and were in accordance with the policies of the NIH Guide for the Care and Use of Laboratory Animals. *Scn1a*^{tm1K^{ea}} mice, containing a deletion of exon 1 of *Scn1a*, were a generous gift from the laboratory of Dr Jennifer Kearney at Northwestern University. The *Scn1a*^{tm1K^{ea}} colony was maintained by breeding heterozygous (129S6.*Scn1a*^{+/-}) animals to 129S6/SvEvTac mice (Taconic #129SVE). To label PV+ FS interneurons, 129S6.*Scn1a*^{+/-} mice were crossed with PV-Cre/tdTom mice on the C57BL/6J background, as in previous work,¹⁶ and subsequently C57BL/6J mice to generate *Scn1a*^{+/-}/PV-Cre/tdTom and *Scn1a*^{+/-}/PV-Cre/tdTom mice on the F1 background. Genotyping of F1 pups was performed by PCR amplification of mouse genomic DNA. Primers used in genotyping were: 5'-AGTCTGTACCAGGCAGAACTTG-3'; 5'-CTGTTTGCTCCATCTTGTCATC-3' and 5'-GCTTTTGAAGCGTGCAGAATGC-3'. The PCR products are 1 kb for the *Scn1a* wild-type allele and 650 bp for the transgenic allele. All mice were maintained on a 12:12 h light:dark cycle and had *ad libitum* access to food and water throughout the experiments. Male and female mice were used in all experiments.

Single bolus intracerebroventricular injection in neonate mice

Lyophilized ASO-84 was reconstituted in 1 × PBS (Thermo Fisher, 10010023) and the concentration of ASO-84 solution was determined by OD₂₆₀ nm absorbance. For ICV injection in P2 mice, pups were immobilized by gentle restraint on a soft tissue padded surface with two fingers. A 33-gauge needle (Hamilton, 7803-05, 0.375-inch long, point style 4, 12° bevelled) attached to a 5 μ l micro-volume syringe (Hamilton, 7634-01) was used for the injection. The coordinates of the injection were ~1 mm lateral and -2 mm ventral from the bregma. ASO-84 (2 μ l for the 20 μ g dose) or PBS was injected slowly into one cerebral lateral ventricle. Injected mice were quickly returned to the nest and observed daily for survival and signs of stress. Investigators performing the injections were blinded to study material and genotype.

Survival analysis

After injection, animals were monitored daily through P90 for survival. Survival data were plotted and analysed as previously described.¹³

Na_v1.1 quantification in mouse brain

Whole brains were collected from surviving mice from the survival analysis 1–3 days after P90. Brain tissue lysates were prepared as previously described.¹³ Na_v1.1 protein was measured using Meso Scale Discovery Immunoassay, as previously described.^{13,17}

RT-qPCR

RNA was isolated from the somatosensory cortex of P17–18 untreated or ASO-injected mice using the Qiagen RNeasy Plus kit according to the manufacturer's instructions. Tissue was homogenized with a Tissue-Tearor (BioSpec Products, Inc.) followed by lysis through a sterile 18-gauge hypodermic needle and vortexing. RNA samples were quantified on a NanoDrop One Spectrophotometer (ThermoFisher Scientific) to ensure adequate concentration and purity and then stored at -80°C. cDNA was generated from 1 μ g of RNA using reverse transcriptase SuperScript III (RT SS III), random primers and dNTPs (Invitrogen). RNA, random primers and dNTPs were incubated at 65°C for 5 min. Salt buffers, 0.1 M DTT, RNase Out and RT SS III were added and reactions were incubated at

25°C for 5 min, 50°C for 60 min, and 70°C for 15 min. Quantitative PCR was performed using SYBR Green (Applied Biosystems) and gene-specific primers (*Scn1b*, *Scn1a*, *Gapdh*; Integrated DNA Technologies) on a QuantStudio 7 Flex Real-Time PCR System (Applied Biosystems). Gene-specific measurements of each cDNA sample were run in triplicate, along with the endogenous control gene *Gapdh* used for normalization, and then compared to wild-type expression levels. The relative expression level of each gene was quantified using the comparative threshold ($2^{-\Delta\Delta C_t}$) method of quantification. Data are presented as the fold change in gene expression \pm standard deviation (SD). Statistical significance ($P < 0.05$) of comparisons between genotypes was determined using Student's *t*-test.

Preparation of brain slices

Acute brain slices were prepared as described.^{16,18–20} In brief, the brain was rapidly removed following euthanasia by isoflurane and decapitation. Coronal brain slices (200–250 μm) containing the somatosensory cortices were prepared from P21–P25 wild-type and *Scn1a*^{+/−} mice in ice-cold, oxygenated slicing solution saturated with 95% O₂/5% CO₂. The slicing solution contained (in mM): 110 sucrose, 62.5 NaCl, 2.5 KCl, 7.5 MgCl₂, 1.25 KH₂PO₄, 26 NaHCO₃, 0.5 CaCl₂ and 20 D-glucose (pH 7.35–7.4 when saturated with 95% O₂/5% CO₂ at 22–25°C). Slices were incubated initially in slicing solution for 10–20 min at room temperature followed by a 1:1 mixture of slicing solution and artificial CSF in a holding chamber aerated continuously with 95% O₂/5% CO₂ at 35°C for 30 min and then room temperature for at least another 30 min before use; artificial CSF contained (in mM): 125 NaCl, 2.5 KCl, 1 MgCl₂, 1.25 KH₂PO₄, 26 NaHCO₃, 2 CaCl₂ and 20 D-glucose (pH 7.35–7.4).

Electrophysiological recording

Whole-cell patch clamp recording methods were detailed in our previous publications.^{16,18–20} Each slice was placed in a recording chamber and superfused (2–4 ml/min) with standard artificial CSF bubbled continuously with 95% O₂/5% CO₂. Individual pyramidal cells or PV+ interneurons in cortical layers 2–6 were visually identified with infrared differential interference contrast (IR-DIC) optics based on size, shape and location or by td-Tomato epifluorescence labelling, respectively, using a NIKON E600FN upright microscope equipped with a Nomarski 40 \times water immersion lens with IR-DIC optics (Nikon Inc.). Recording electrodes were fire polished and had a resistance of 3–7 M Ω depending on the pipette solutions filled. The whole cell current-clamp recording technique was used to record APs and firing patterns of individual PV+ interneurons in slices. The whole-cell voltage-clamp recording technique was used to examine GABAergic spontaneous inhibitory postsynaptic currents (sIPSCs) in pyramidal cells in slices. For recording of APs, recording electrodes had a resistance of 4–7 M Ω when filled with a K-gluconate based pipette solution that consisted of (in mM): 140 K-gluconate, 4 NaCl, 0.5 CaCl₂, 10 HEPES, 5 EGTA, 2 Mg-ATP, 0.4 GTP and 5 phosphocreatine (pH 7.2–7.3, adjusted with KOH). Repetitive AP firing was evoked by injections of a series of 1500 ms currents varying from –60 to 300 pA at 10 pA steps from their resting membrane potentials (RMPs) or a holding potential of –65 mV. Individual APs were evoked by injections of 1 ms threshold depolarizing currents while the individual cells were held at RMP or –65 mV. Minimum currents required for the initiation of APs were assessed by a Rheobase protocol (a series of 300 ms currents stepping from –10 pA in 1 pA increments until APs were evoked consistently). After completion of AP recordings,

spontaneous excitatory postsynaptic currents (sEPSCs) were recorded from the same neurons in the presence or absence of 10 μM bicuculline (Sigma-Aldrich) at a holding potential of –70 mV, as previously described.²⁰ With this low [Cl[−]] containing internal solution and a holding potential of –70 mV, which is close to the predicted equilibrium potential for Cl[−] (–83 mV), all inward currents were predicted to be glutamate receptor-mediated and bicuculline-insensitive. In the presence of bicuculline, neurons often generated huge inward sodium currents corresponding to spontaneous AP firing. For this reason, sEPSCs shown in figures are selected from sections of recordings lacking AP firing.

For recording sIPSCs in cortical layer 2–6 pyramidal cells, the pipette solution consisted of (in mM) 140 CsCl, 0.4 GTP, 2 Mg-ATP, 0.5 CaCl₂, 5 Na₂Phosphocreatine; 5 EGTA-CsOH, 10 HEPES (pH 7.3 adjusted with CsOH). With almost symmetric [Cl[−]] inside and outside of the cells, all inward currents were presumably GABAergic when the cells were held at –70 mV and in the presence of 6-Cyano-7-nitroquinoxaline-2,3-dione (CNQX, 10 μM) and amino-5-phosphonopentanoic acid (APV, 100 μM) in the external solution to block glutamate receptor-mediated sEPSCs. Signals were amplified with a Multiclamp 700B amplifier (Molecular Devices), filtered at 2–6 kHz and digitized at 20 kHz for offline analysis. Data were acquired with a Digidata 1440A interface and analysed using pClamp10 or 11 (Molecular Devices, Sunnyvale, CA, USA). All experiments were carried out at room temperature (22°C–25°C).

Acute isolation of cortical PV+ interneurons

Cortical PV+ interneurons were acutely isolated, as previously described.¹⁶ Brain slices were prepared as above and maintained at room temperature until dissociation. Somatosensory cortex was isolated via microdissection using a 26.5-gauge needle under a dissection microscope. Tissues were incubated at 35°C in oxygen saturated Hanks' balanced salt solution (HBSS) supplemented with 10 mM HEPES with 1.5 mg/ml protease type XIV (Sigma) for 16 min. Tissue was washed three times with oxygen saturated ice-cold low-calcium HBSS (1:10 HBSS with calcium and magnesium: HBSS calcium- and magnesium-free) containing 10 mM HEPES. HBSS was replaced with ice-cold, oxygen saturated Na-isethionate solution (in mM; 140 Na-isethionate, 23 glucose, 15 HEPES, 2 KCl, 4 MgCl₂, 0.1 CaCl₂) and tritiated with fire polished glass Pasteur pipettes to suspend cells. Cells were allowed to settle on a glass coverslip for 10 min prior to recording. All recordings were acquired <1.5 h post-dissociation. PV+ cells were identified by td-Tomato epifluorescence. Cells lacking neurites were not selected for recording.

Sodium current recordings

Sodium current was measured at room temperature using the standard whole-cell patch clamp technique with previously described electrophysiological protocols.¹⁶ Cells were superfused with external sodium channel recording solution containing (in mM): 30 NaCl, 1 BaCl₂, 2 MgCl₂, 45 CsCl, 0.2 CdCl₂, 1 CaCl₂, 10 HEPES, 20 TEA-Cl and 100 D-glucose (pH 7.35 adjusted with CsOH, osmolarity 300–305 mOsm). Micropipettes were obtained from 1.5 mm outer diameter capillary glass tubing (Warner Instruments) using a P-2000 horizontal puller (Sutter Instrument Co.). Micropipettes were polished using a MF-830 microforge (Narishige) to obtain a resistance of 2–4 M Ω . Pipettes were filled with intracellular solution that contained the following (in mM): 1 NaCl, 125 N-methyl-D-glucamine, 2 MgCl₂, 10 EGTA, 40 HEPES, 5 phosphocreatine-tris, 2 Mg-ATP, 0.2 Na₂-GTP, 0.1 leupeptin

(osmolarity 270–275 mOsm, pH 7.2 adjusted with H₂SO₄). Signals were amplified using a Multiclamp 700B amplifier (Molecular Devices). Data were acquired with a Digidata 1440A interface (Molecular Devices) and analysed using pClamp10 offline. Pipette and whole-cell capacitance were fully compensated, and series resistance was predicted and compensated 40–50% when needed. Signals were low pass-filtered at 10 kHz and data were sampled at 20 kHz. Residual linear capacity and leak currents were eliminated using online P/4 subtraction. Holding potential was –80 mV and a 250 ms prepulse to –120 mV was applied for all protocols.

Electrophysiological data analysis

Brain slice electrophysiological data analysis was performed as described previously.^{16,18–20} The cell passive membrane electrical properties, AP firing patterns, and kinetics were analysed using Clampfit 10 or 11 (Molecular Devices, Sunnyvale, CA, USA). Spontaneous synaptic currents were screened automatically using MiniAnalysis 6.0.3 (Synaptosoft Inc.) with a set of the prespecified parameters and then accepted or rejected manually based on kinetic properties with event detection amplitude, area thresholds and shape of the spontaneous events. Unless otherwise specified, synaptic events per cell collected over a 2-min period were averaged to calculate the mean frequency and amplitude of spontaneous synaptic currents. Amplitudes of currents were measured after subtraction of the baseline noise. Only individual sIPSCs with a clear stable and smooth baseline, fast rise phase from a flat baseline and complete decay without interruption were selected for kinetic analysis. Synaptic events with spike overlap or absence of a clear baseline were excluded. At least 100 events per cell were averaged for kinetic analysis. Peak current amplitudes were measured at the absolute maximum after subtraction of baseline noise. sIPSC decay times were measured as the time required for the current to decay from 10% to 90% of the peak amplitude. The decay phase was best fitted with a bi-exponential function using the curve fitting program provided by MiniAnalysis software. All results were plotted in GraphPad Prism (GraphPad; La Jolla, CA, USA). Data are presented as mean value ± SEM, where *n* or *N* are numbers of cells or animals, respectively. Statistical significance was determined using two-way ANOVA with *post hoc* multiple comparisons or unpaired Student's *t*-test unless stated otherwise. Data with *P* < 0.05 were deemed significant.

Data analysis of the recorded sodium current was performed using the software packages Clampfit v10.7 (Molecular Devices), Microsoft Excel and SigmaPlot 14.5 (Systat Software). Results are presented as mean ± SEM unless indicated otherwise.

Immunofluorescence labelling

Wild-type and *Scn1a*^{+/-} mice at P22 or P27 (untreated) and P22 or P27 (ASO-84-treated) were anaesthetized with isoflurane and transcardially perfused with PBS followed by 1% paraformaldehyde. Brains were dissected, postfixed overnight in 1% paraformaldehyde, sequentially submerged overnight in 10% and 30% sucrose, then flash-frozen in O.C.T. and stored at –80°C until use. Coronal sections (20 μm) were generated on a Leica CM1850 cryostat and stored at –20°C until use. Immunofluorescence labelling was performed as previously described.¹⁶ Briefly, slides were rehydrated in 0.05 M phosphate buffer (PB) and blocked for at least 2 h in blocking solution (10% normal goat serum and 0.3% Triton X-100 in 0.1 M PB). Slides were incubated in primary antibodies in blocking buffer overnight at room temperature. The next day, slides were washed 3 × 10 min with 0.1 M PB, incubated with

secondary antibodies in blocking buffer for 2 h, washed 3 × 10 min in 0.1 M PB, then mounted with ProLong Gold + DAPI and stored at 4°C until imaging.

Primary antibodies: guinea pig anti-parvalbumin (Synaptic Systems 195 004, 1:500), rabbit anti-ankyrin-G (a gift from Dr Paul Jenkins, University of Michigan, 1:500), rabbit anti-Cux1 (Proteintech 11733-1-AP, 1:250) or rabbit anti-Foxp2 (Abcam ab16046, 1:500). Secondary antibodies: Alexa Fluor-488 goat anti-rabbit or Alexa Fluor-568 goat anti-guinea pig (Invitrogen).

Fluorescent images were acquired on a Nikon A1R confocal system with a Nikon FN1 microscope using a 20 × 0.75 NA objective and Nikon NIS-Elements AR software. Images were acquired at matched locations relative to bregma in somatosensory cortex. Three images per mouse per cortical layer [for axon initial segment (AIS) analysis] and six images per mouse per cortical layer (for PV+ interneuron quantification) were analysed using NIH ImageJ. Graphs were generated and statistical analysis was performed using GraphPad Prism 9.4. AIS lengths and numbers of PV+ interneurons were compared across genotypes and age/treatment groups using two-way ANOVA with multiple *post hoc* comparisons. Figures were assembled in Adobe Photoshop 2023.

Results

ASO-84 increases *Scn1a* mRNA and Na_v1.1 protein and reduces SUDEP in Dravet syndrome mice

ASO-84 targets splicing of human SCN1A exon 20N, similar to ASO-22, which we described previously.^{13,21} Here, we used ASO-84 as a surrogate for ASO-22. To demonstrate the pharmacology and efficacy of ASO-84, we tested the effects of ASO-84 on SUDEP incidence in the *Scn1a*^{Tm^{Kea}} (F1:129S.*Scn1a*^{+/-} × C57BL/6J) mouse model of Dravet syndrome, in which exon 1 of *Scn1a* is deleted, resulting in haploinsufficiency.²² These mice typically have a ~50% rate of premature mortality due to SUDEP,²² although this rate is known to vary between different laboratories and mouse facilities. In Fig. 1A, vehicle (PBS, purple) or a single, 20 μg dose of ASO-84 (blue) was ICV-injected in one brain hemisphere of wild-type or *Scn1a*^{+/-} littermates at P2 and survival was monitored until P90. Kaplan-Meier analysis showed that ASO-84 injection resulted in survival of 92% of *Scn1a*^{+/-} Dravet syndrome mice (23 of 25 survived, blue solid line) up to 90 days compared to survival of 60% of littermate Dravet syndrome mice treated with PBS during this period (15 of 25 survived, solid purple line, *P* < 0.01). Ninety-seven per cent of wild-type mice (28 of 29 survived, dashed purple line) dosed with PBS survived during the same period. Figure 1B (purple: PBS, blue: ASO-84) shows that *Scn1a* mRNA abundance in brains isolated from surviving P90 ASO-84-treated wild-type and *Scn1a*^{+/-} mice was increased ~1.5-fold compared to those treated with PBS. Figure 1C (purple: PBS, blue: ASO-84) shows that the expression level of Na_v1.1 protein in brains isolated from surviving P90 ASO-84-treated wild-type mice was increased ~2-fold compared to those treated with PBS. The expression level of Na_v1.1 protein in brains of surviving P90 ASO-84-treated *Scn1a*^{+/-} mice was not significantly different from the level measured in brains of PBS-treated wild-type mice at P90. Despite the increased expression of Na_v1.1 protein in the brains of ASO injected wild-type animals, there was no impact on survival over the 90-day period (Fig. 1A, dashed blue line), similar to our previous result with ASO-22.¹³

Previous work showed reduced VGSC β1 subunit protein, encoded by *Scn1b*, in several brain regions of adult *Scn1a*^{Tm^{Kea}}

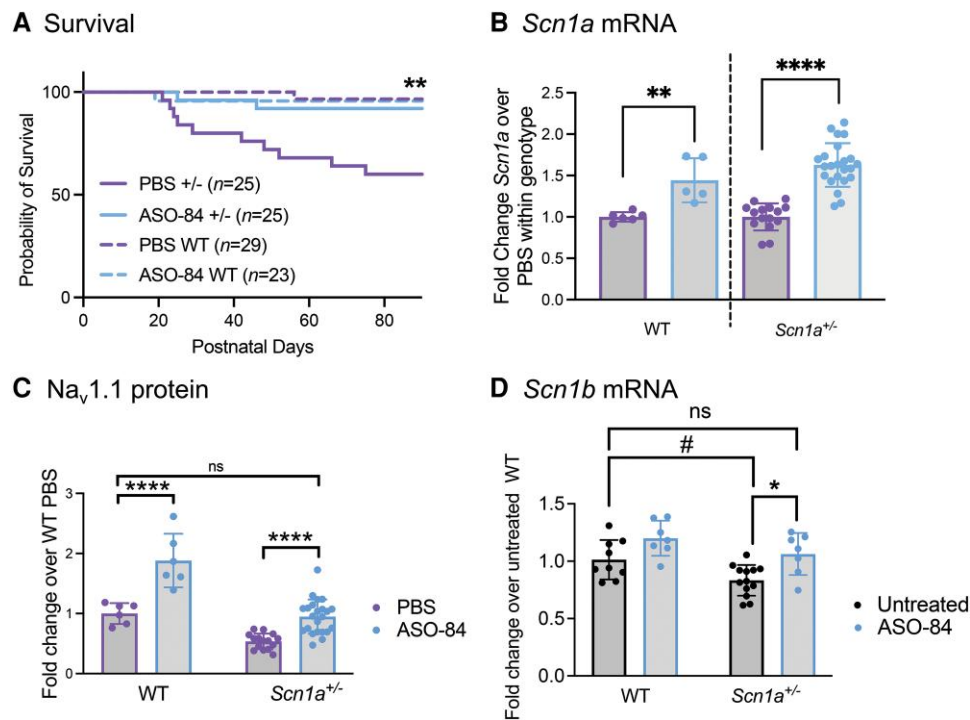


Figure 1 A single intracerebroventricular dose of ASO-84 at P2 reduces SUDEP in *Scn1a*^{+/-} mice, increases *Scn1a* mRNA and Na_v1.1 protein in wild-type and *Scn1a*^{+/-} mouse brains, and increases *Scn1b* expression in *Scn1a*^{+/-} somatosensory cortex. (A) A single intracerebroventricular (ICV) dose of ASO-84 at P2 significantly improved survival of *Scn1a*^{+/-} mice (solid blue) compared to PBS-treated *Scn1a*^{+/-} mice (solid purple) through P90 (***P* = 0.0088). Dashed purple: PBS-treated wild-type (WT) mice. Dashed blue: ASO-84-treated wild-type mice. Kaplan-Meier (Wilcoxon) analysis. (B) A single dose of ASO-84 at P2 (blue bars) significantly increased *Scn1a* mRNA abundance in P90 wild-type and *Scn1a*^{+/-} mouse brains compared to PBS treatment (purple bars). ***P* < 0.0005; *****P* < 0.0001. Data are presented as mean ± standard deviation (SD). Each data-point represents an independent sample from one animal. Unpaired Student's *t*-tests were used to compare each ASO-treated genotype to its PBS control set to 1. (C) A single dose of ASO-84 at P2 (blue bars) significantly increased Na_v1.1 protein in P90 wild-type and *Scn1a*^{+/-} mouse brains compared to PBS treatment (purple bars). *****P* < 0.0001; ns = no significant change. Data are presented as mean ± SD. Each data-point represents an independent sample from one animal. Two-way ANOVA followed by Tukey's multiple comparisons test was used for comparison of means between independent groups. (D) A separate group of untreated animals showed a trending decrease in *Scn1b* mRNA expression in *Scn1a*^{+/-} somatosensory cortex compared to wild-type mice (black bars, #*P* = 0.059). A single dose of ASO-84 at P2 (blue bars) significantly increased *Scn1b* mRNA in P17–18 *Scn1a*^{+/-} mouse somatosensory cortex compared to untreated (black bars) *Scn1a*^{+/-} cortex. The level of *Scn1b* mRNA expression in ASO-84-treated *Scn1a*^{+/-} cortex was not significantly different from the level measured in untreated wild-type cortex. Each data-point represents an independent sample from one animal. Untreated WT: *n* = 9, ASO-84-treated WT: *P* = 7, untreated *Scn1a*^{+/-}: *n* = 13, ASO-84-treated *Scn1a*^{+/-}: *n* = 7. **P* < 0.05; ns = no significant change (one-way ANOVA followed by Tukey's multiple comparisons test). Data are presented as mean ± SD, with *n* equal to the number of independent samples from individual animals. SUDEP = sudden unexpected death in epilepsy.

(F1:129S.*Scn1a*^{+/-}×C57BL/6J) Dravet syndrome mice.²³ Here, we performed RT-qPCR in a separate group of animals to compare *Scn1b* mRNA abundance in untreated wild-type and *Scn1a*^{+/-} mouse brain (Fig. 1C, black). We found a trending decrease in *Scn1b* mRNA expression in *Scn1a*^{+/-} cortex compared to wild-type mice (black, *P* = 0.059). A single dose of ASO-84 at P2 (blue bars) significantly increased *Scn1b* mRNA in P17–18 *Scn1a*^{+/-} mouse somatosensory cortex compared to untreated (black bars) *Scn1a*^{+/-} cortex. Importantly, the level of *Scn1b* mRNA expression in ASO-84-treated *Scn1a*^{+/-} cortex was not significantly different from the level measured in untreated wild-type cortex, suggesting that ASO treatment restored this effect in the Dravet syndrome model.

Dravet syndrome PV+ cortical interneurons have a lower threshold for action potential firing and are more sensitive to depolarization block

To determine whether ASO-84 treatment at P2 impacts the excitability of pyramidal neurons or PV+ fast-spiking interneurons, we generated *Scn1a*^{+/-}/PV-Cre/tdTomato and *Scn1a*^{+/-}/PV-Cre/tdTomato mice on the 129S6×C57BL/6J F1 background to facilitate visualization of PV neurons by epifluorescence, similar to Kaneko

et al.²⁴ We compared the AP firing properties of wild-type and *Scn1a*^{+/-} pyramidal neurons, identified using IR-DIC optics, or PV+ interneurons, identified by epifluorescence, in the somatosensory cortical regions of acute brain slices at P21–25. Figure 2A shows representative traces recorded from wild-type (black) or *Scn1a*^{+/-} (blue) cortical layer 2/3 PV+ interneurons in brain slices, respectively. Figure 2B summarizes the input-output (I–O) curves for AP firing in response to current injections for all recorded PV+ cells (25 cells each from 17 wild-type or 14 *Scn1a*^{+/-} mice). *Scn1a*^{+/-} PV+ interneurons required less depolarizing current injection to initiate AP firing (Fig. 2A, right) compared to wild-type (Fig. 2A, left). In this example, a 30 pA current injection was sufficient to initiate AP firing in a layer 2/3 *Scn1a*^{+/-} interneuron, whereas a 60 pA current injection was required to evoke AP firing in a layer 2/3 wild-type interneuron. We found that *Scn1a*^{+/-} PV+ interneurons fired significantly more APs in the lower range of depolarizing current injection than did wild-type interneurons, indicating hyperexcitability (Fig. 2A and B). As current injection intensities increased, *Scn1a*^{+/-} interneurons fired significantly fewer APs and became sensitive to depolarization-induced block compared to wild-type interneurons (Fig. 2A and B). In contrast to PV+ interneurons, pyramidal neurons showed no differences in intrinsic excitability between genotypes.

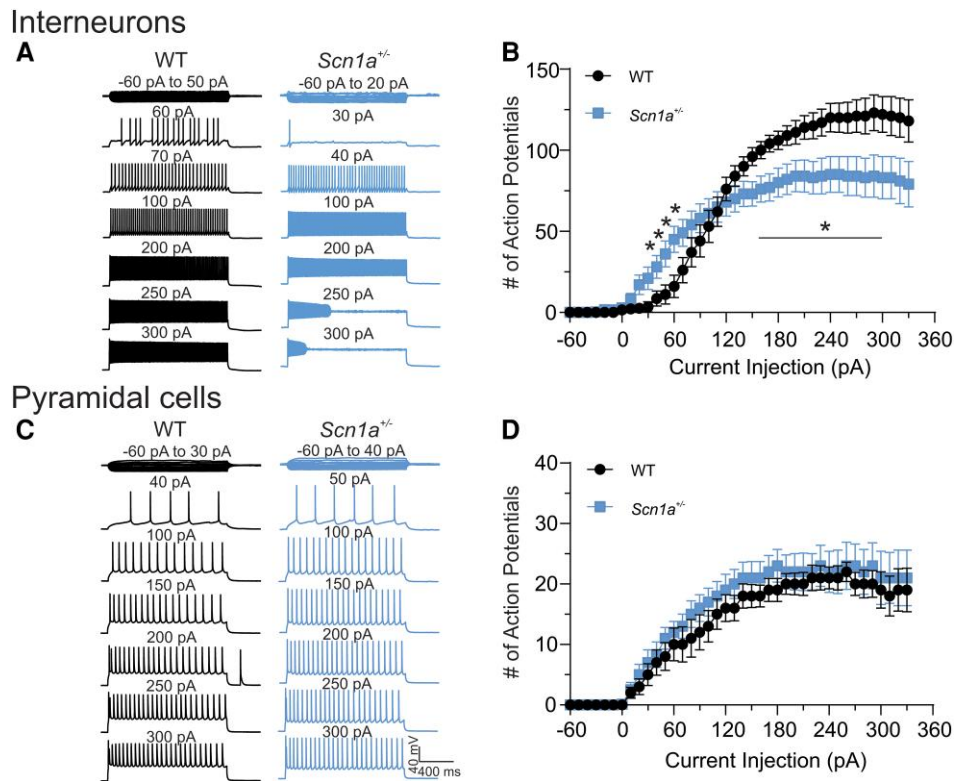


Figure 2 *Scn1a*^{+/-} PV+ interneurons, but not pyramidal neurons, show stimulation intensity-dependent biphasic changes in excitability. (A) Representative traces showing evoked repetitive firing of fast spiking PV+ interneurons in cortical layer 2/3 of brain slices from P21–25 wild-type (WT) (black) or *Scn1a*^{+/-} (blue) mice. Repetitive action potential (AP) firing was evoked by injections of 1500 ms currents from –60 to 330 pA (selected responses are shown) at 10 pA-step from their resting membrane potentials. Here, a representative *Scn1a*^{+/-} interneuron began to fire APs at lower intensities of current injection compared to the representative wild-type interneuron. Stronger depolarizing current injections blocked repetitive firing in the *Scn1a*^{+/-} interneuron. (B) Input-output (I–O) curves for AP firing of wild-type versus *Scn1a*^{+/-} PV+ interneurons in response to current injections. I–O curves were generated by plotting the number of evoked APs by 1500 ms current injections against current intensities over a range of –60 to 330 pA. (C) Representative traces showing evoked repetitive firing of pyramidal neurons in cortical layer 2/3 of brain slices from wild-type (black) or *Scn1a*^{+/-} (blue) mice. Repetitive AP firing was evoked by injections of 1500 ms currents from –60 to 330 pA (selected responses are shown) at 10 pA-step from their resting membrane potentials. (D) I–O curves for AP firing of wild-type versus *Scn1a*^{+/-} pyramidal neurons in response to current injections. I–O curves were generated by plotting the number of evoked APs by 1500 ms current injections against current intensities over a range of –60 to 330 pA. Values are mean ± standard error of the mean (SEM) of 25 cells from 15 wild-type mice or 26 cells from 13 *Scn1a*^{+/-} mice, respectively. *Significant differences between wild-type and *Scn1a*^{+/-} mice ($P < 0.01$). PV = parvalbumin.

Figure 2C shows representative traces recorded from wild-type (black) or *Scn1a*^{+/-} (blue) cortical layer 2/3 pyramidal neurons in brain slices. Figure 2D summarizes the I–O curves for AP firing in response to current injections for all recorded cells.

Our data show clearly that *Scn1a* haploinsufficiency affects the excitability of PV+ fast-spiking interneurons, similar to previous work showing that $\text{Na}_v1.1$ is the predominant sodium channel α -subunit expressed in this cell population.²⁵ Importantly, *Scn1a* mRNA is also expressed in pyramidal neurons,²⁶ and thus the excitability of this cell population could be affected by ASO-84 administration. To test this hypothesis, we asked whether the excitability of pyramidal neurons was altered in Dravet syndrome mice. Results presented in Fig. 2C and D showed that the AP firing patterns and cumulative I–O curves for wild-type and *Scn1a*^{+/-} pyramidal neurons were not statistically different, suggesting no changes in excitability in this cell population. Supplementary Table 3 summarizes the results of sEPSC recordings from wild-type and *Scn1a*^{+/-} PV+ interneurons in cortical brain slices. We found no differences in the average values for sEPSC amplitude or frequency between genotypes in the presence or absence of ASO-84 treatment, suggesting that cortical pyramidal neuron input to PV+ interneurons is unchanged.

ASO-84 treatment restores the firing pattern of cortical PV+ Dravet syndrome interneurons in brain slices

We compared the AP firing patterns of P21–25 wild-type and *Scn1a*^{+/-} PV+ interneurons following a single ICV dose of ASO-84 or vehicle at P2 (Fig. 3). Figure 3A shows representative traces of evoked repetitive firing from cortical layer 2/3 PV+ interneurons in brain slices from wild-type (black) or *Scn1a*^{+/-} (blue) mice following ASO-84 administration. In contrast to untreated interneurons (Fig. 2), ASO-84-treated wild-type and *Scn1a*^{+/-} interneurons showed similar AP firing patterns in response to current injections. Figure 3B compares I–O curves of AP firing for ASO-84-treated wild-type versus *Scn1a*^{+/-} PV+ interneurons. In contrast to Fig. 2B, showing initial hyperexcitability followed by hypoexcitability and depolarization block of untreated Dravet syndrome PV+ interneurons, these data show no differences between genotypes. Figure 4 summarizes the neuronal firing results for all treatments and genotypes. PBS treatment resulted in no significant changes in AP firing patterns compared to untreated interneurons of either genotype (Fig. 4A and B, PBS-treated purple, untreated black). ASO-84 treatment had no significant effects on the firing pattern of wild-type interneurons compared to untreated

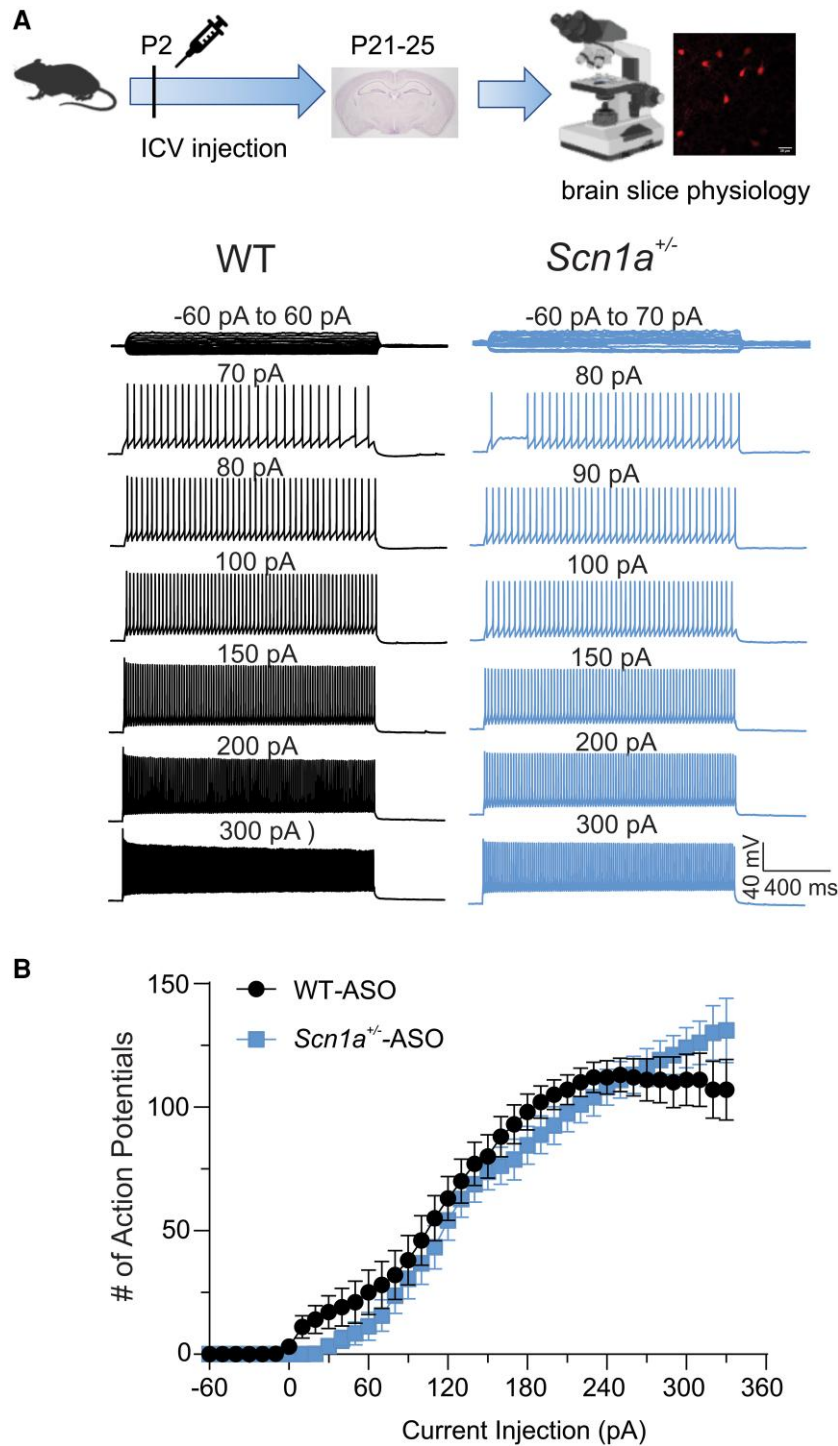


Figure 3 A single dose of ASO-84 restores neuronal excitability of *Scn1a*^{+/-} PV+ interneurons. *Top*: Study design. (A) Representative traces showing evoked repetitive firing of cortical layer 2/3 PV+ interneurons in slices from P21–25 wild-type (WT) (black) or *Scn1a*^{+/-} (blue) mice following one dose of ASO-84 at P2. Repetitive action potential (AP) firing was evoked using the same protocol, as described in Fig. 2. Here, wild-type and *Scn1a*^{+/-} interneurons showed similar AP firing patterns in response to current injections. (B) Input-output (I–O) curves for AP firing of wild-type versus *Scn1a*^{+/-} PV+ interneurons following ASO-84 treatment. Values are mean ± standard error of the mean (SEM) of 24 cells from 13 wild-type mice or 19 cells from 12 *Scn1a*^{+/-} mice, respectively. Study design panel generated with BioRender. ASO = antisense oligonucleotide; ICV = intracerebroventricular; PV = parvalbumin.

or PBS-treated (Fig. 4A, blue). In contrast, ASO-84 treatment increased the minimum depolarizing currents required for AP initiation, shifting the I–O curve to the right, and reduced sensitivity to depolarization block for *Scn1a*^{+/-} interneurons compared to untreated and

PBS-treated interneurons, thus normalizing their excitability (Fig. 4B, blue).

Figure 4C–F separate the PV+ interneuron data, shown in Fig. 4A and B, by sex. Figure 4C and D show results for untreated and

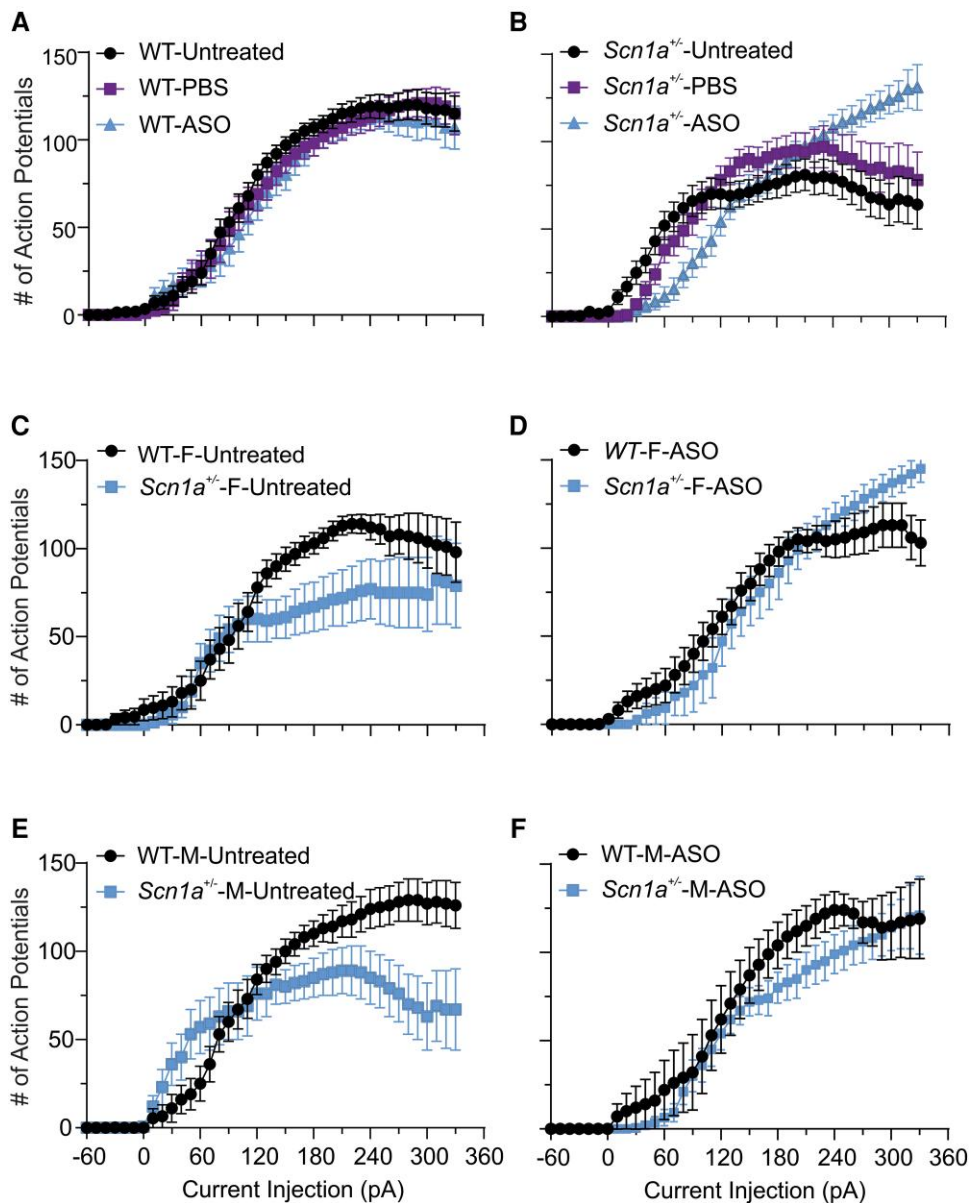


Figure 4 (Single-dose ASO-84 injection at P2 restores neuronal excitability of *Scn1a*^{+/-} PV+ interneurons. (A and B) Comparisons of input-output (I-O) curves for action potential (AP) firing of P21–25 wild-type (WT) or *Scn1a*^{+/-} PV+ interneurons without or with PBS or single-dose ASO-84 treatment. (A) PBS or ASO-84 had no significant effects on AP firing patterns of wild-type PV+ interneurons. (B) PBS injection did not affect the AP firing pattern of *Scn1a*^{+/-} PV+ interneurons. Single-dose ASO-84 treatment eliminated the stimulation intensity-dependent biphasic changes in excitability and sensitivity to depolarization block of *Scn1a*^{+/-} PV+ interneurons. Black = untreated neurons; purple = PBS-treated neurons; blue = ASO-84-treated neurons. Values are mean ± standard error of the mean (SEM) of 15–25 cells from 8–15 wild-type mice or 19–26 cells from 8–13 *Scn1a*^{+/-} mice, respectively. (C–F) Sex differences in PV+ interneuron firing patterns and ASO effects: (C) AP firing of PV+ interneurons from female *Scn1a*^{+/-} mice (*Scn1a*^{+/-}-F-untreated) showed a higher sensitivity to depolarization block compared to those from female wild-type mice (WT-F). (D) Single-dose ASO-84 treatment eliminated the difference in sensitivity of AP firing to depolarization-induced block in PV+ interneurons between female wild-type (WT-ASO) and *Scn1a*^{+/-} mice (*Scn1a*^{+/-}-F-ASO). (E) AP firing of PV+ interneurons from male *Scn1a*^{+/-} mice (*Scn1a*^{+/-}-M-untreated) showed stimulation intensity-dependent early hyperexcitability and late higher sensitivity to depolarization block compared to those from male wild-type mice (WT-M). (F) Single-dose ASO-84 treatment eliminated the difference in the early hyperexcitability and later sensitivity of AP firing to depolarization-induced block in PV+ interneurons between male wild-type (WT-M-ASO) and *Scn1a*^{+/-} mice (*Scn1a*^{+/-}-M-ASO). Values are mean ± SEM of 10 cells from six untreated female wild-type mice and 15 cells from 10 female *Scn1a*^{+/-} mice, respectively. Values in C are mean ± SEM of 10 cells from six untreated female wild-type mice and 15 cells from 10 untreated female *Scn1a*^{+/-} mice. Values in D are mean ± SEM of 16 cells from eight ASO-84-treated female wild-type mice and eight cells from six female *Scn1a*^{+/-} mice. Values in E are mean ± SEM of 15 cells from 10 untreated male wild-type mice and 14 cells from nine untreated male *Scn1a*^{+/-} mice. Values in F are mean ± SEM of seven cells from four ASO-84-treated male wild-type mice and 11 cells from five male *Scn1a*^{+/-} mice. PV = parvalbumin.

ASO-84-treated female wild-type (black) and *Scn1a*^{+/-} (blue) mice, respectively. Figure 4E and F show results for untreated and ASO-84-treated male wild-type (black) and *Scn1a*^{+/-} (blue) mice, respectively. Interestingly, when separated by sex, the initial

hyperexcitability observed for untreated *Scn1a*^{+/-} PV+ interneurons is evident in male (Fig. 4F), but not female (Fig. 4C), animals. Importantly however, ASO treatment normalized the excitability of PV+ interneurons from mice of both sexes (Fig. 4D and F).

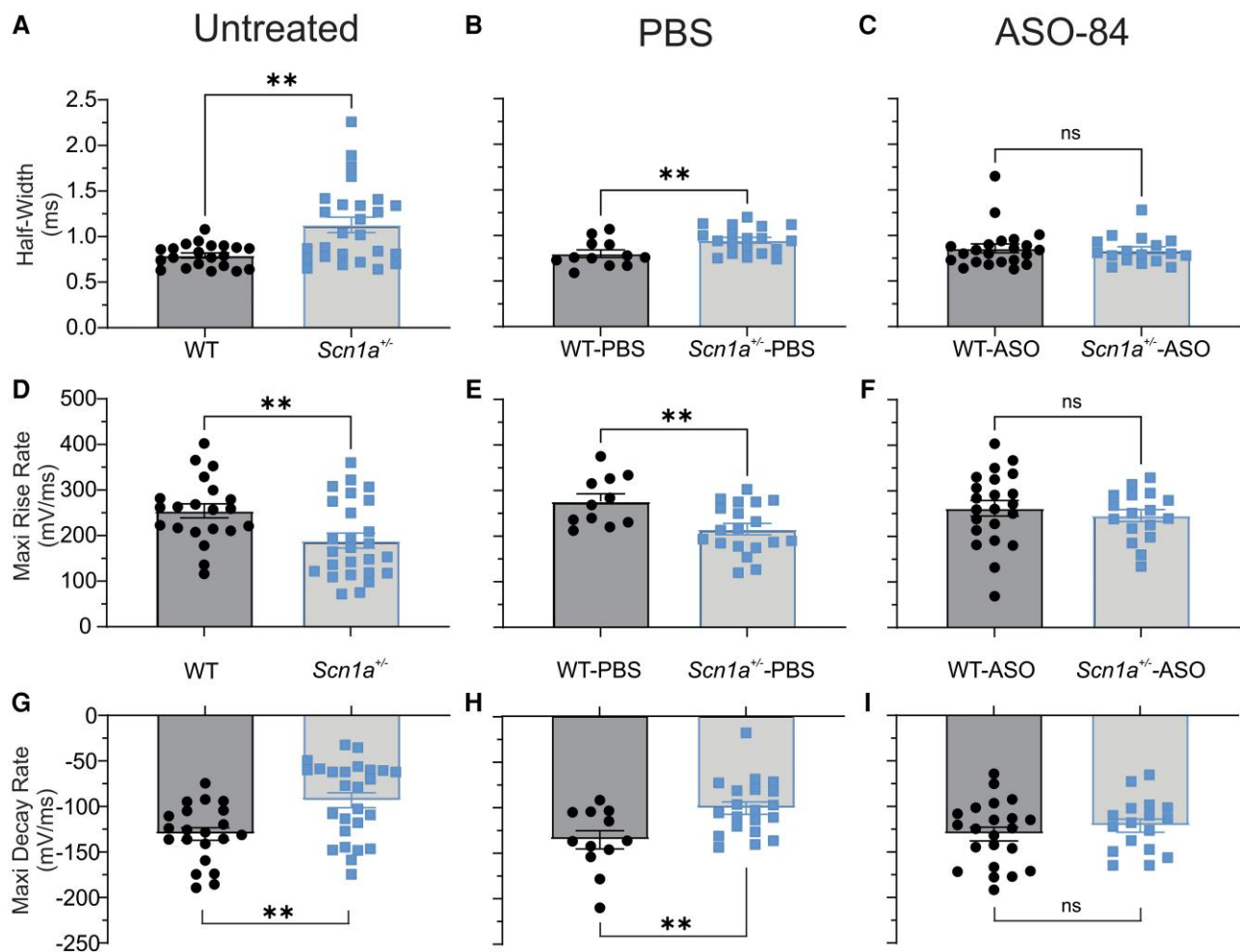


Figure 5 Single-dose ASO-84 treatment restores action potential waveform and kinetics of *Scn1a*^{+/-} PV+ interneurons. (A–C) Comparison of action potential (AP) duration (half-width) of untreated, PBS-treated or ASO-84-treated wild-type (WT) or *Scn1a*^{+/-} P21–25 PV+ interneurons, respectively. (D–F) Comparison of maximum rise rates of APs of untreated, PBS-treated or ASO-84-treated wild-type or *Scn1a*^{+/-} PV+ interneurons, respectively. (G–I) Comparison of maximum decay rates of APs of untreated, PBS-treated or ASO-84-treated wild-type or *Scn1a*^{+/-} PV+ interneurons, respectively. Values are mean ± standard error of the mean (SEM) of 11–21 cells from 8–12 wild-type mice or 17–24 cells from 11–12 *Scn1a*^{+/-} mice. WT = black; *Scn1a*^{+/-} = blue. *Significant differences between wild-type and *Scn1a*^{+/-} PV+ interneurons ($P < 0.01$). Results are tabulated in [Supplementary Table 1](#). ns = not significant; PV = parvalbumin.

Figure 5 compares the AP kinetic properties of P21–25 untreated, PBS-treated and ASO-84-treated PV+ interneurons. All results are summarized in [Supplementary Table 1](#). Untreated ([Fig. 5A, D and G](#) and [Supplementary Table 1](#)) and PBS-treated ([Fig. 5B, E and H](#) and [Supplementary Table 1](#)) *Scn1a*^{+/-} PV+ interneurons had significantly prolonged AP durations, slower maximum rising rates and slower maximum decay rates compared to wild-type. These differences were resolved following ASO-84 treatment ([Fig. 5C, F and I](#) and [Supplementary Table 1](#)). We found no significant differences in RMP or peak AP amplitude between genotypes with or without ASO treatment ([Supplementary Table 1](#)). There were no significant differences in membrane capacitance between genotypes in the absence of ASO treatment. ASO-84 treatment increased the membrane capacitance of wild-type and *Scn1a*^{+/-} interneurons, although only the increase in *Scn1a*^{+/-} neurons was significant ([Supplementary Table 1](#)). Finally, there were no significant differences in input resistance, threshold potential or minimal current required for AP initiation between wild-type and *Scn1a*^{+/-} interneurons, regardless of treatment ([Supplementary Table 1](#)).

Cortical Dravet syndrome pyramidal neurons show reduced spontaneous inhibitory post-synaptic current frequency

We predicted that PV+ interneuron hypoexcitability over the range of high frequency stimulation would result in decreased presynaptic GABA release. To test this hypothesis, we recorded GABAergic sIPSCs in cortical pyramidal cells located adjacent to td-Tomato-labelled PV+ interneurons in brain slices. [Figure 6A](#) shows representative sIPSCs recorded from untreated wild-type (black) or *Scn1a*^{+/-} (blue) layer 2/3 pyramidal neurons. The cumulative distribution of sIPSC frequency recorded from these untreated neurons is shown in [Fig. 6C](#) and the cumulative amplitudes are shown in [Fig. 6E](#). Taken together, the data in [Fig. 6A, C and E](#), showing reduced frequency but not amplitude, suggest that GABA release is impaired in *Scn1a*^{+/-} interneurons. [Figure 6B](#) shows representative sIPSCs recorded from ASO-84-treated wild-type (black) or *Scn1a*^{+/-} (blue) layer 2/3 pyramidal neurons. [Figure 6D](#) shows cumulative distributions of sIPSC frequency and [Fig. 6F](#)

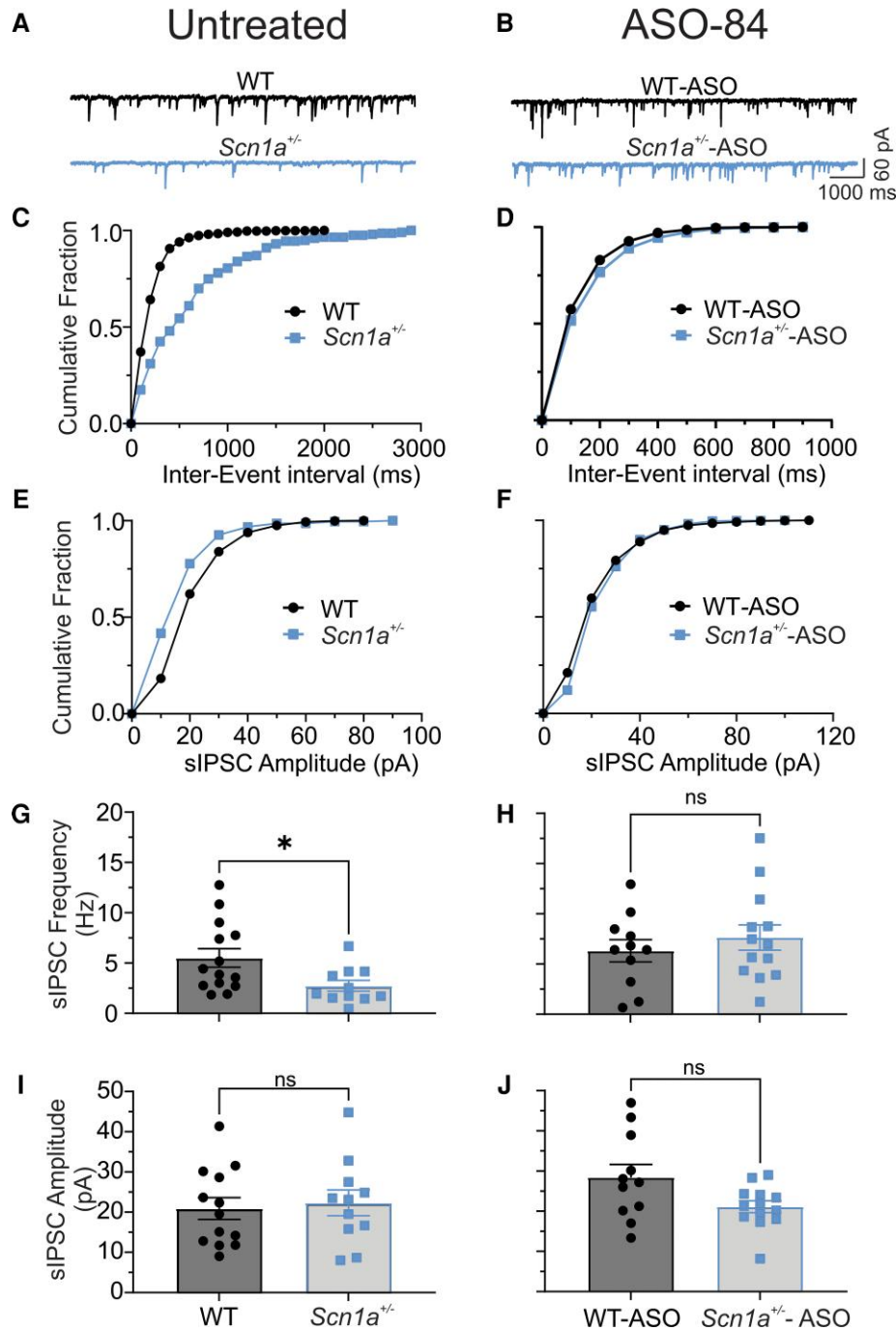


Figure 6 *Scn1a*^{+/-} cortical pyramidal neurons have reduced sIPSC frequency, but not amplitude. A single dose of ASO-84 restores GABAergic synaptic function. Spontaneous inhibitory-evoked currents (sIPSCs) were recorded from a holding potential of -70 mV in the presence of 10 μM CNQX and 100 μM APV. (A and B) Representative traces showing sIPSCs recorded from cortical layer 2/3 P21-25 wild-type (WT) (black) or *Scn1a*^{+/-} (blue) pyramidal cells adjacent to PV+ interneurons without (left) or with ASO-84 (right) treatment, respectively. (C and E, D and F) Comparisons of cumulative fraction of inter-event intervals and amplitudes of sIPSCs from the same cells shown in A and B. In the absence of ASO-84 treatment, each trace or value is representative of recordings from 15 cells of eight WT mice or 11 cells of five *Scn1a*^{+/-} mice, respectively. With ASO-84 treatment, each trace or value is a representative example of recordings from eight cells of four WT mice or 11 cells of four *Scn1a*^{+/-} mice, respectively. (G and H) Comparison of mean sIPSC frequencies recorded from cortical layer 2-4 WT or *Scn1a*^{+/-} pyramidal cells, respectively. (I and J) Comparison of sIPSC amplitudes recorded from cortical layer 2-4 WT or *Scn1a*^{+/-} pyramidal cells, respectively. Values are mean ± standard error of the mean (SEM) of eight cells from four WT mice or 11 cells from four *Scn1a*^{+/-} mice. *P < 0.05. ns = not significant; PV = parvalbumin.

shows cumulative amplitudes of these neurons. Importantly, ASO-84 treatment normalized the cumulative sIPSC frequency distribution curves of *Scn1a*^{+/-} cells to that of wild-type. Figure 6G and H and Supplementary Table 2 summarize the mean frequency of

sIPSCs recorded from cortical pyramidal neurons in the absence (Fig. 6G) or presence (Fig. 6H) of ASO-84 treatment. Figure 6I and J and Supplementary Table 2 summarize the mean amplitude of sIPSCs recorded from cortical pyramidal neurons in the absence

(Fig. 6I) or presence (Fig. 6J) of ASO-84 treatment. The frequency of sIPSCs recorded from *Scn1a*^{+/-} pyramidal cells was significantly lower than in wild-type pyramidal cells, with no significant differences in sIPSC amplitude between genotypes, reflecting the reduced neuronal excitability observed in *Scn1a*^{+/-} PV+ interneurons. ASO-84 treatment normalized this difference in sIPSC frequency between genotypes. These results are consistent with the observed restoration of PV+ interneuron firing following ASO treatment. Kinetic analysis of sIPSC decay τ s showed no differences between genotypes (Supplementary Table 2).

Cortical PV+ Dravet syndrome interneurons have reduced sodium current density that is increased by ASO-84 treatment

Yu et al.²⁵ demonstrated that acutely dissociated P14 *Scn1a*^{+/-} GABA+ hippocampal neurons with bipolar morphology had reduced sodium current density compared to wild-type neurons. Mistry et al.²⁷ repeated this observation in P14–15 *Scn1a*^{+/-} hippocampal GABAergic neurons identified by combined Patch-seq and morphology criteria. This important early work led to the development of the disinhibition hypothesis underlying the mechanism of Dravet syndrome. However, while PV+ fast-spiking interneurons have been implicated as primary drivers of the Dravet syndrome mechanism,²⁸ there are no reports in the literature showing specific changes in sodium current density in genetically labelled PV+ interneurons in a Dravet syndrome mouse model. Here, we measured sodium current density from P21–25 acutely dissociated wild-type and *Scn1a*^{+/-} cortical PV+ interneurons labelled with tdTomato epifluorescence. Neurons were acutely dissociated from the same brain slice preparations used for current clamp recordings. Figure 7A shows representative families of sodium current traces measured in voltage clamp mode for untreated wild-type, untreated *Scn1a*^{+/-} and ASO-84-treated *Scn1a*^{+/-} cortical PV+ interneurons. We found that sodium current density was reduced by approximately half in *Scn1a*^{+/-} cortical PV+ interneurons. ASO-84 administration at P2 restored the level of sodium current density in P21–25 *Scn1a*^{+/-} cortical PV+ interneurons to that of untreated wild-type neurons. Figure 7B quantifies sodium current density data from multiple experiments. Sodium current density of *Scn1a*^{+/-} PV+ interneurons was ~50% of that measured in wild-type, reflecting *Na_v1.1* haploinsufficiency. ASO-84 treatment increased sodium current density in wild-type PV+ neurons above control, consistent with the increased *Na_v1.1* protein expression in the brain shown in Fig. 1. Most importantly, the level of sodium current density in ASO-84 treated PV+ *Scn1a*^{+/-} interneurons was statistically indistinguishable from that measured in PV+ cells isolated from untreated wild-type animals, showing that ASO-84 treatment restores sodium current density in cortical fast-spiking interneurons in Dravet syndrome mice. In contrast to changes in sodium current density, we found no changes in sodium current voltage-dependent properties between genotypes or treatments (Supplementary Table 4).

Interneuron axon initial segment length is not altered in Dravet syndrome mice

Previous work has suggested that adaptive changes in the length of the AIS can fine-tune neuronal excitability and modulate plasticity in response to activity or neurological disease.²⁹ We measured AIS lengths in P22 and P27 wild-type and *Scn1a*^{+/-} layer 2 and layer 6 somatosensory cortical neurons with and without ASO-84 treatment. Brain slices were labelled with anti-PV antibody to identify

fast-spiking interneurons, anti-ankyrin-G to identify the AIS, anti-Cux1 to label cells in cortical layer 2/3, or anti-Foxp2 to label cells in cortical layer 6. Supplementary Fig. 1 shows that there were no significant differences in PV+ interneuron AIS length between genotypes or ages in layer 2 (Supplementary Fig. 1A–C) or layer 6 (Supplementary Fig. 1D–F). Furthermore, ASO-84 administration had no effect on AIS length in either genotype. Supplementary Table 5 summarizes data for mean AIS lengths for all neurons and for PV+ neurons specifically in layers 2 and 6.

Layer-specific localization of PV+ interneurons

GABAergic signalling influences the migration of newborn cortical neurons as they progress from deep to superficial cortical layers during brain development.³⁰ Because we observed reduced GABAergic signalling in Dravet syndrome cortical slices, we hypothesized that PV+ neuronal migration might also be altered. We compared PV+ interneuron cell body density in layers 2/3 (Supplementary Fig. 1G–I) versus layer 6 (Supplementary Fig. 1J–L) in wild-type versus *Scn1a*^{+/-} mouse brain slices as a surrogate measure of neuronal migration. In each image, the areas demarcated by anti-Cux1 or anti-Foxp2 are indicated by dotted lines, with Cux1+ or Foxp2+ neurons shown in the first panel of Supplementary Fig. 1G and J and in Supplementary Fig. 2. At P22 and P27, we counted fewer PV+ neurons per 500 μm^2 in *Scn1a*^{+/-} layer 2/3 slices compared to wild-type, suggesting that fewer cells migrated into superficial layers from deep cortical layers at these time points. ASO-84 treatment restored *Scn1a*^{+/-} PV+ neuron numbers relative to wild-type at both ages. We observed age-dependent increases in PV+ neuron density in layer 6 in both genotypes reflecting ongoing brain development. ASO-84 treatment resulted in a transient increase followed by a reduction in layer 6 PV+ neuron density in *Scn1a*^{+/-} slices.

Discussion

Dravet syndrome is a catastrophic DEE that is largely caused by pathogenic variants in *SCN1A* resulting in haploinsufficiency of the VGSC α -subunit *Na_v1.1*.⁵ While some anti-seizure therapies^{10,11} provide partial seizure management for some patients with Dravet syndrome, they do not affect the complex set of Dravet syndrome comorbidities.⁶ Thus, there is a significant need for novel approaches to target *SCN1A* haploinsufficiency using gene-modifying strategies.⁶ Toward that goal, we showed previously that a single ICV dose of STK-001 (ASO-22), generated using TANGO technology to prevent inclusion of the NMD exon 20N in human *SCN1A*, increased productive *Scn1a* transcript and *Na_v1.1* expression and reduced the incidence of electrographic seizures and SUDEP in a *Scn1a*^{+/-} mouse model of Dravet syndrome.¹³ We proposed that STK-001 may have therapeutic benefit for Dravet syndrome patients with *SCN1A* variants that result in haploinsufficiency. Here, we investigated the mechanism of action of ASO-84, a surrogate for ASO-22 that also targets splicing of exon 20N, in *Scn1a*^{+/-} Dravet syndrome mouse brain. Using a similar administration protocol as in our previous work,¹³ we tested the effects of a single ICV injection of ASO-84 in one brain hemisphere at P2. Our results show that administration of ASO-84 at P2 results in long-lasting increases in brain *Na_v1.1* protein in both wild-type and Dravet syndrome mice and prolongs survival in Dravet syndrome mice, similar to ASO-22.¹³

Homozygous mice expressing the null allele of *Scn1b*, encoding sodium channel β 1 subunits, also model Dravet syndrome.³¹ We demonstrated that *Scn1b*^{-/-} somatosensory cortex is haploinsufficient

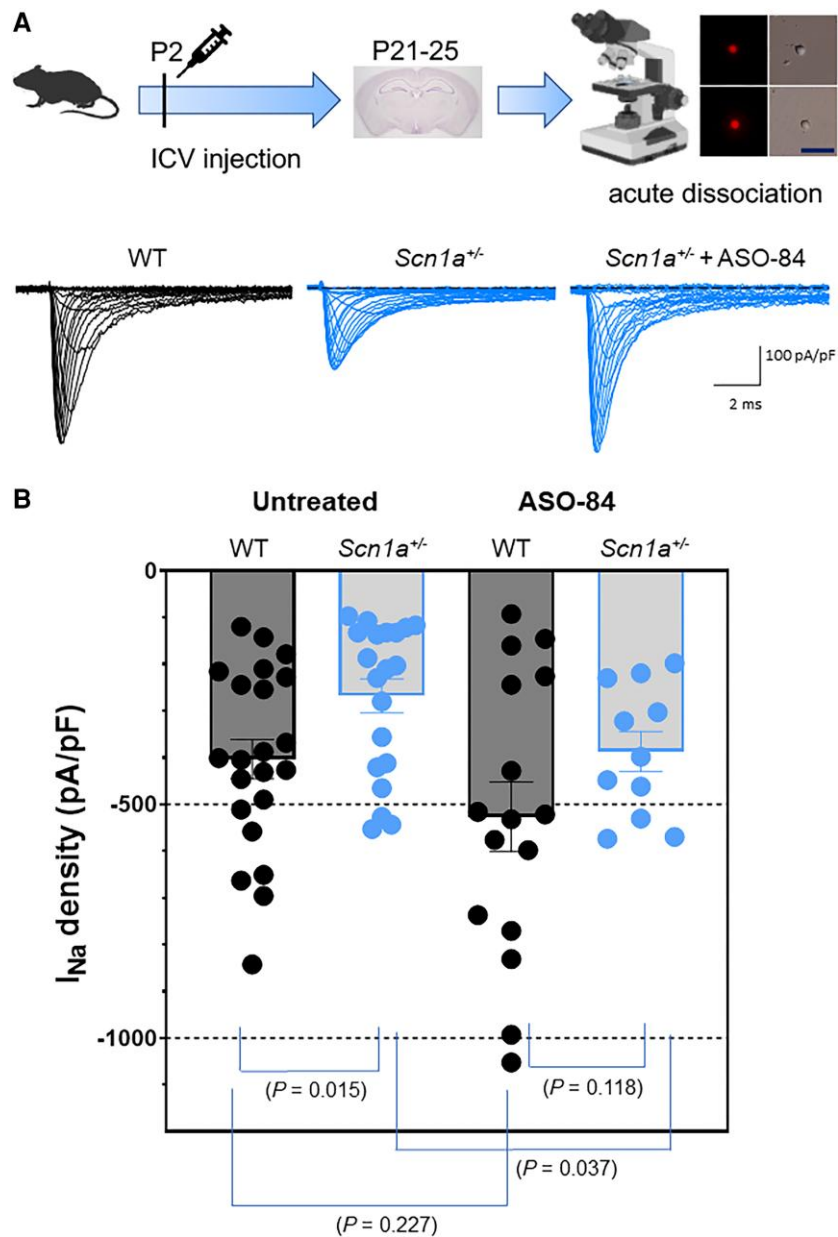


Figure 7 A single dose of ASO-84 at P2 restores sodium current density in acutely dissociated *Scn1a*^{+/-} PV+ interneurons recorded at P21–25. Top: Study design including a representative image of a brain slice under epifluorescence to show acutely dissociated PV+ interneurons. Scale bar = 25 μ m. (A) Representative sodium current families evoked by 250 ms depolarizing pulses from -100 to +20 mV with 5 and 10 mV steps, from one untreated wild-type (WT) neuron (black), one untreated *Scn1a*^{+/-} neuron (blue, middle) or one ASO-84-treated *Scn1a*^{+/-} neuron (blue, right). All traces show sodium current density with the same scale. (B) Maximum sodium current density for untreated neurons (left) for WT (*n* = 22) and *Scn1a*^{+/-} (*n* = 20), *P* = 0.018; and for neurons treated with ASO-84 (right) for WT (*n* = 16) and *Scn1a*^{+/-} (*n* = 11), *P* = 0.118. All comparison *P*-values are indicated in the figure. Study design panel generated with BioRender.

for *Scn1a* at P17–18³² and that P17–18 *Scn1b*^{-/-} cortical PV+ interneurons are hypoexcitable.¹⁶ Conversely, *Scn1a* Dravet syndrome mice have been shown to express reduced levels of sodium channel β 1 subunit protein in several brain areas.²³ Here, we found that untreated *Scn1a*^{+/-} Dravet syndrome mice have a nearly significant (*P* = 0.059) reduction in *Scn1b* mRNA abundance in somatosensory cortex compared to wild-type at P17–18. Administration of ASO-84 at P2 normalized this value in *Scn1a*^{+/-} Dravet syndrome mice assessed at P17–18 but did not significantly impact *Scn1b* mRNA abundance in wild-type brain. Taken together, these results suggest that *Scn1a* and *Scn1b* may play synergistic roles in Dravet syndrome mouse

models and that ASO-84 treatment can normalize compensatory gene expression effects resulting from *Scn1a* haploinsufficiency. These results also suggest that ASO-84 treatment results in increased levels of functional, heterodimeric ($\alpha + \beta$ 1) Na_v1.1 channels in brain.

We demonstrate that, in untreated mice, intrinsic AP firing properties of Dravet syndrome cortical pyramidal neurons are unchanged compared to controls at P21–25. In contrast, sodium current density is reduced compared to controls in Dravet syndrome PV+ interneurons while AP firing properties are biphasic, showing initial hyperexcitability at low current injections followed by depolarization block at high levels of current injection. IPSC frequency

recorded from cortical pyramidal neurons is reduced in untreated Dravet syndrome mice, suggesting reduced GABA release from interneurons resulting in disinhibition. A single dose of ASO-84 at P2 restored excitability and sodium current density in PV+ Dravet syndrome interneurons and restored GABAergic signalling to Dravet syndrome cortical pyramidal neurons recorded at P21–25. PV+ neuron AIS lengths were unchanged in P22–27 untreated *Scn1a*^{+/-} layer 2 and layer 6 cortex compared to wild-type controls, suggesting that AIS plasticity does not contribute to alterations in excitability over this time period. This result contrasts with previous data showing elongation of *Scn1a*^{+/-} PV+ neuron AIS lengths; however, the cortical region and layer positioning of those neurons may have been different than the present work.³³ While mean AIS lengths were shorter in Favero *et al.*³³ compared to our results, our results agree with other published measurements in mouse visual cortex.³⁴ We found that the density of PV+ neurons in superficial cortical layers 2/3 was reduced, suggesting possible neuronal migration delays during development of Dravet syndrome mouse brain, similar to previous observations in *Scn1b*^{-/-} mice, which also model Dravet syndrome.³⁵ ASO-84 treatment reversed this reduction in neuronal density at both ages. In deep cortical layer 6, age-dependent increases in PV+ neuron density occurred in both genotypes; however, ASO-84 treatment led to a larger transient increase in neuron density at P22, possibly contributing to the density changes in layers 2/3. Taken together, this new work provides critical mechanistic information for further development of precision medicine approaches to treat patients with SCN1A-linked Dravet syndrome and related DEEs.

Previous work demonstrated that STK-001 (ASO-22) modestly, but significantly, increased the excitability of somatosensory cortical layer 5 PV+ interneurons in Dravet syndrome mice but reduced PV+ neuronal excitability in wild-type mice.³⁶ No differences were detected between vehicle-treated wild-type and vehicle-treated Dravet syndrome PV+ interneurons in terms of in RMP, input resistance, AP threshold, AP amplitude, downstroke velocity, or AP duration. Vehicle-treated Dravet syndrome PV+ interneurons were observed to have reduced AP upstroke velocity relative to wild-type; however, this reduction was not rescued by ASO-22 treatment. There are several notable differences between the previous study and the present work. Here, we show that untreated and vehicle-treated Dravet syndrome PV+ interneurons are hyperexcitable in the lower range of depolarization stimulation and then become hypoexcitable in the higher range of depolarizing current injections due to depolarization-induced block (Figs 2 and 4), similar to the original report of hippocampal GABAergic neurons in Dravet syndrome mice.²⁵ ASO-84 treatment restores these excitability differences in Dravet syndrome cortical PV+ neurons but does not affect wild-type neurons. Importantly, neither the initial hyperexcitability nor depolarization block were observed in Dravet syndrome PV+ interneurons in,³⁶ likely due to the use of 500 ms depolarizing current pulses to induce AP firing, which would have required injection of stronger depolarizing currents to induce depolarization block. In contrast, the AP protocol used here included longer 1500 ms depolarizing pulses, which induced depolarization block at lower levels of current injection. In contrast to Wengert *et al.*,³⁶ our results show significant differences in passive and active membrane electrical properties between genotypes that are restored following ASO-84 treatment, including input resistance, AP rise rate, AP decay rate and AP duration. These changes provide a mechanistic explanation as to why Dravet syndrome PV+ interneurons fire fewer APs than wild-type. In addition, increased input resistance may contribute to PV+ interneuron hyperexcitability in the lower range of

depolarizing current injections because less current is required to evoke an AP. Differences in brain area studied, as well as sizes of experimental groups between the two studies may also be important. The previous study³⁶ examined only cortical layer 5 neurons while we examined cells from cortical layers 2–6 but focused primarily on layer 2/3 interneurons. In addition, the previous study reported experimental *n* values of 22–32 cells from three mice per genotype or treatment. In our work, no more than three cells from each mouse were included for analysis and at least 10 mice were used per group, allowing wider sampling of individual animals.

Early experimental work in *Scn1a* Dravet syndrome mouse models demonstrating selective loss of sodium current density in GABAergic, but not glutamatergic, neurons in brain during the second postnatal week led to the hypothesis that the primary mechanism of SCN1A-linked Dravet syndrome is disinhibition.²⁵ Subsequent work implicated PV+ fast-spiking interneurons as primary targets in Dravet syndrome pathology,^{28,37,38} although other interneuron subtypes, e.g. somatostatin+ and VIP+, clearly play roles in the mechanism of disease.^{28,39} Recent work by Goldberg and colleagues used an innovative mini-slice procedure in live mice to assess PV+ neuronal excitability in Dravet syndrome mice that undergo SUDEP versus those that survive.²⁴ These authors showed that P16–21 *Scn1a*^{+/-} Dravet syndrome mice that later underwent SUDEP had a similar biphasic PV+ interneuron I-O relationship as we found for untreated P21–25 Dravet syndrome mice (Fig. 2B). In their hands, P16–21 *Scn1a*^{+/-} Dravet syndrome mice that later did not undergo SUDEP did not show the initial hyperexcitability. Because our experimental design did not allow for determination of which untreated Dravet syndrome animals would succumb to SUDEP, we are not able to directly compare our results with the previous work²⁴; however, this possibility will be important to investigate further in the future, as it may present novel areas for therapeutic intervention as well as a possible biomarker for increased SUDEP risk.

Sex is an important biological variable in epilepsy.^{40,41} While male patients show a higher risk of developing epilepsy as a whole, females are more frequently diagnosed with idiopathic, or genetic, generalized epilepsies than males, although sociological stigmatization may influence reporting of seizures to physicians in some populations.⁴⁰ In a study of patients with idiopathic generalized epilepsy, the mean age of seizure onset was found to be 1.3 years earlier in males compared to females. However, myoclonic seizures were more frequently reported by females and photoparoxysmal responses in the EEG laboratory were more often observed in females.⁴² In patients with combined epilepsy and intellectual disability, higher mortality risk was observed in females, which remained significantly elevated after adjusting the data for sociodemographic factors and developmental or congenital disorders.⁴³ In contrast, male sex has been associated with a 1.4-fold increased risk for SUDEP in combined case-control studies.⁴⁴ There are limited studies reporting the effects of sex differences on clinical outcomes in patients with Dravet syndrome. Cetica *et al.*⁴⁵ analysed SCN1A mutation type and seven parameters available at clinical presentation, including sex, family history of epilepsy, age at seizure onset, type and duration of first seizure, fever at first seizure, and epileptiform discharges at first EEG in predicting Dravet syndrome versus milder outcomes in 182 mutation carriers ascertained after seizure onset; however, sex was not found to be a significant prognostic factor between groups. For the F1. *Scn1a*^{tm1K^{ea}} Dravet syndrome mouse model used here, previous work by Hampson and colleagues showed that female mice display a higher rate of mortality than males.²³ This result was confirmed by the Henshall group⁴⁶ as well as the Kearney group.⁴⁷ In the conditional F/+;Meox2-Cre⁺ mouse model of Dravet syndrome,

males and females were similarly impacted by the *Scn1a* mutation, except that males were observed to be more susceptible to social interaction deficits.⁴⁸ Importantly, we show that ASO-84 is equally effective in male and female mice, thus STK-001 is predicted to provide therapeutic benefit to male and female Dravet syndrome patients.

Interestingly, while ASO treatment significantly increased Na_v1.1 protein expression in wild-type brain as well as sodium current density in acutely dissociated wild-type PV+ interneurons, the neuronal firing properties investigated in ASO-treated wild-type brain slices were not different from untreated animals. Taken together, these results suggest that excess Na_v1.1 channels above a certain set point in the PV+ neuronal cell body do not impact AP firing properties and that the density of sodium channels at the PV+ interneuron AIS do not change in ASO-treated wild-type animals. In contrast, ASO treatment corrected Na_v1.1 haploinsufficiency in Dravet syndrome brain, restored Dravet syndrome PV+ interneuron sodium current density in acutely dissociated neurons and restored PV+ interneuron AP firing properties in Dravet syndrome cortical brain slices, implying that the mechanism of Na_v1.1 channel targeting in PV+ neurons may be different in Dravet syndrome brains compared to wild-type. We attempted to address this hypothesis using confocal immunofluorescence techniques to study the subcellular localization of Na_v1.1 channels in Dravet syndrome and wild-type brain slices. Unfortunately, currently available anti-Na_v1.1 antibodies are not of sufficient quality to perform this experiment. Future work, perhaps using a mouse model expressing epitope-tagged Na_v1.1 channels, will be necessary to solve this puzzle. Identification of Dravet syndrome variants in genes that encode Na_v1.1 targeting proteins may suggest novel therapeutic approaches. For example, recent work showed that viral-mediated overexpression of VGSC β1 subunits, which are known to chaperone VGSC α-subunits to the plasma membrane,⁴⁹ has modest effects on mortality and behaviour in *Scn1a*^{+/-} Dravet syndrome mice.²³

NMD, or poison, exons are naturally occurring, premature termination codon containing, alternative exons that are thought to play important roles in developmental regulation as well as cell type specificity of gene expression.⁵⁰ Exon 20N is critical for the regulation of *Scn1a* expression during normal brain development. We showed previously that exon 20N-containing *Scn1a* transcript is expressed at low levels early in postnatal mouse brain development and remains constant at least through to 10 months of age.¹³ In contrast, productive *Scn1a* transcript that does not contain exon 20N begins to increase around P6 and plateaus around P14, becoming the predominant *Scn1a* transcript as the brain continues to develop.¹³ In 1998, Oh and Waxman showed that inclusion of exon 20N prevents the generation of functional Na_v1.1 channels in astrocytes, thus regulating the cell type specificity of Na_v1.1 expression in the brain.⁵¹ Exon 20N also plays a role in pathophysiology. Carvill and colleagues reported five likely pathogenic Dravet syndrome patient variants in exon 20N that promote its inclusion, supporting the hypothesis that these variants lead to epilepsy through reduction of full-length *SCN1A* mRNA and Na_v1.1 protein.¹⁴ Generation of a knock-in mouse model of one of these patient variants, NM_006920.4(*SCN1A*):c.3969 + 2451G > C, tested this hypothesis. *Scn1a*^{KI/+} mice showed an approximate 50% reduction in full-length *Scn1a* mRNA and Na_v1.1 protein levels in the brain, premature mortality, and hyperactivity with occasionally observed spontaneous seizures.¹⁵ RT-qPCR studies showed that ~1% of *Scn1a* mRNA in brains from wild-type mice aged 1.9–19 months include exon 20N. In contrast, brain tissue from age-matched knock-in mice showed an approximate 5-fold increase in the extent of exon 20N inclusion. Analysis of a previously generated RNA-seq data set obtained from wild-type mouse cortex showed that levels

of exon 20N inclusion were ~70% at E14.5, suggesting its importance in embryonic brain development.¹⁵

Our work suggests that TANGO ASOs may provide an effective therapeutic strategy for patients with Dravet syndrome caused by *SCN1A* variants that result in Na_v1.1 haploinsufficiency. Recent studies have demonstrated that other neurological diseases of haploinsufficiency may benefit from a similar approach. An assessment of public variant databases showed that a large proportion of pathogenic variants have viable avenues for ASO therapy, including TANGO.⁵² In addition to *SCN1A*, several other genes are disease-associated and harbour NMD exons that may be amenable to TANGO manipulation.⁵² For example, variants in *SYNGAP1* that result in NMD are linked to intellectual disability, autism and schizophrenia.⁵³ Most *SYNGAP1* patients also suffer from epileptic seizures.⁵³ An alternative 3' splice site in *SYNGAP1* induces NMD in mouse and human neural development.⁵⁴ Deletion of this *Syngap1* splice site in mice upregulated *Syngap1* protein and alleviated the long-term potentiation and membrane excitability deficit phenotype of *Syngap1* null mice. Development of a splice-switching oligonucleotide that converted the *SYNGAP1* unproductive isoform to the functional form in human induced pluripotent stem cell-derived neurons gives preclinical support for this potential therapeutic approach.⁵⁴ In conclusion, emerging ASO technologies are providing novel gene-modifying therapeutic strategies to treat the underlying mechanisms of DEE and related neurological diseases. This novel precision medicine approach may transform the standard of care for these otherwise intractable diseases.

Data availability

Data will be made available by the corresponding author upon reasonable request.

Funding

Funded by National Institutes of Health (NIH) NS076752 to L.L.I., a grant from Stoke Therapeutics to L.L.I., NIH U54NS117170 to L.L.I. (postdoctoral funding for S.L.H.), the Vivian L. Cotton Epilepsy Research Fund to L.L.I., and a University of Michigan Department of Pharmacology Centennial Graduate Fellowship to N.D.

Competing interests

A.C., S.J. and Z.H. were employees of Stoke Therapeutics at the time this work was completed. A portion of the work was funded by a grant from Stoke Therapeutics to the Regents of the University of Michigan.

Supplementary material

Supplementary material is available at *Brain* online.

References

1. Dravet C, Bureau M, Bernardina BD, Guerrini R. Severe myoclonic epilepsy in infancy (Dravet syndrome) 30 years later. *Epilepsia*. 2011;52(Suppl 2):1-2.
2. Wirrell EC, Hood V, Knupp KG, et al. International consensus on diagnosis and management of Dravet syndrome. *Epilepsia*. 2022; 63:1761-1777.

3. Bureau M, Genton P, Delgado-Escueta A, Dravet C, Guerrini R, Tassinari CA, Thomas P, Wolf P, eds. *Epileptic syndromes in infancy, childhood and adolescence*. John Libby EUROTEXT; 2019.
4. Guerrini R, Aicardi J. Epileptic encephalopathies with myoclonic seizures in infants and children (severe myoclonic epilepsy and myoclonic-astatic epilepsy). *J Clin Neurophysiol*. 2003;20:449-461.
5. Dravet C. The core Dravet syndrome phenotype. *Epilepsia*. 2011; 52(Suppl 2):3-9.
6. Isom LL, Knupp KG. Dravet syndrome: Novel approaches for the most common genetic epilepsy. *Neurotherapeutics*. 2021;18: 1524-1534.
7. Berg AT, Gaebler-Spira D, Wilkening G, et al. Nonseizure consequences of Dravet syndrome, KCNQ2-DEE, KCNB1-DEE, Lennox-Gastaut syndrome, ESES: A functional framework. *Epilepsy Behav*. 2020;111:107287.
8. Cooper MS, McIntosh A, Crompton DE, et al. Mortality in Dravet syndrome. *Epilepsy Res*. 2016;128:43-47.
9. Wu YW, Sullivan J, McDaniel SS, et al. Incidence of Dravet Syndrome in a US Population. *Pediatrics*. 2015;136:e1310-e1315.
10. He Z, Li Y, Zhao X, Li B. Dravet syndrome: Advances in etiology, clinical presentation, and treatment. *Epilepsy Res*. 2022;188:107041.
11. Lopez JC, Pare JR, Blackmer AB, Orth LE. Treatment-refractory Dravet syndrome: Considerations for novel medications. *J Pediatr Health Care*. 2022;36:479-488.
12. Lim KH, Han Z, Jeon HY, et al. Antisense oligonucleotide modulation of non-productive alternative splicing upregulates gene expression. *Nat Commun*. 2020;11:3501.
13. Han Z, Chen C, Christiansen A, et al. Antisense oligonucleotides increase *Scn1a* expression and reduce seizures and SUDEP incidence in a mouse model of Dravet syndrome. *Sci Transl Med*. 2020;12:eaaz6100.
14. Carvill GL, Engel KL, Ramamurthy A, et al. Aberrant inclusion of a poison exon causes dravet syndrome and related SCN1A-associated genetic epilepsies. *Am J Hum Genet*. 2018;103: 1022-1029.
15. Voskobiynyk Y, Battu G, Felker SA, et al. Aberrant regulation of a poison exon caused by a non-coding variant in a mouse model of *Scn1a*-associated epileptic encephalopathy. *PLoS Genet*. 2021; 17:e1009195.
16. Hull JM, O'Malley HA, Chen C, et al. Excitatory and inhibitory neuron defects in a mouse model of *Scn1b*-linked EIEE52. *Ann Clin Transl Neurol*. 2020;7:2137-2149.
17. Han Z, Christiansen A, Meena, Liau G. Relative quantification of Na(V)1.1 protein in mouse brains using a meso scale discovery-electrochemiluminescence (MSD-ECL) method. *Bio Protoc*. 2021;11:e3910.
18. Brackenbury WJ, Yuan Y, O'Malley HA, Parent JM, Isom LL. Abnormal neuronal patterning occurs during early postnatal brain development of *Scn1b*-null mice and precedes hyperexcitability. *Proc Natl Acad Sci U S A*. 2013;110:1089-1094.
19. Lopez-Santiago LF, Yuan Y, Wagnon JL, et al. Neuronal hyperexcitability in a mouse model of SCN8A epileptic encephalopathy. *Proc Natl Acad Sci U S A*. 2017;114:2383-2388.
20. Yuan Y, O'Malley HA, Smaldino MA, Bouza AA, Hull JM, Isom LL. Delayed maturation of GABAergic signaling in the *Scn1a* and *Scn1b* mouse models of Dravet Syndrome. *Sci Rep*. 2019;9:6210.
21. Aznarez I, Han Z, inventors; Stoke Therapeutics, assignee. Antisense oligomers for treatment of conditions and diseases. US patent application 16/561960. 23 January 2020.
22. Miller AR, Hawkins NA, McCollom CE, Kearney JA. Mapping genetic modifiers of survival in a mouse model of Dravet syndrome. *Genes Brain Behav*. 2014;13:163-172.
23. Niibori Y, Lee SJ, Minassian BA, Hampson DR. Sexually divergent mortality and partial phenotypic rescue after gene therapy in a mouse model of Dravet syndrome. *Hum Gene Ther*. 2020; 31(5-6):339-351.
24. Kaneko K, Currin CB, Goff KM, et al. Developmentally regulated impairment of parvalbumin interneuron synaptic transmission in an experimental model of Dravet syndrome. *Cell Rep*. 2022;38: 110580.
25. Yu FH, Mantegazza M, Westenbroek RE, et al. Reduced sodium current in GABAergic interneurons in a mouse model of severe myoclonic epilepsy in infancy. *Nat Neurosci*. 2006; 9:1142-1149.
26. Du J, Simmons S, Brunklaus A, et al. Differential excitatory vs inhibitory SCN expression at single cell level regulates brain sodium channel function in neurodevelopmental disorders. *Eur J Paediatr Neurol*. 2020;24:129-133.
27. Mistry AM, Thompson CH, Miller AR, Vanoye CG, George AL, Kearney JA. Strain- and age-dependent hippocampal neuron sodium currents correlate with epilepsy severity in Dravet syndrome mice. *Neurobiol Dis*. 2014;65:1-11.
28. Tai C, Abe Y, Westenbroek RE, Scheuer T, Catterall WA. Impaired excitability of somatostatin- and parvalbumin-expressing cortical interneurons in a mouse model of Dravet syndrome. *Proc Natl Acad Sci U S A*. 2014;111:E3139-E3148.
29. Huang CY-M, Rasband MN. Axon initial segments: Structure, function, and disease. *Ann N Y Acad Sci*. 2018;1420:46-61.
30. Wang DD, Kriegstein AR. Defining the role of GABA in cortical development. *J Physiol*. 2009;587(Pt 9):1873-1879.
31. Chen C, Westenbroek RE, Xu X, et al. Mice lacking sodium channel beta1 subunits display defects in neuronal excitability, sodium channel expression, and nodal architecture. *J Neurosci*. 2004;24:4030-4042.
32. Chen C, Ziobro J, Robinson-Cooper L, et al. Epilepsy and SUDEP in a mouse model of human SCN1B-linked developmental and epileptic encephalopathy. *Brain Commun*. 2023;5(6):fcad283
33. Favero M, Sotuyo NP, Lopez E, Kearney JA, Goldberg EM. A transient developmental window of fast-spiking interneuron dysfunction in a mouse model of Dravet syndrome. *J Neurosci*. 2018;38:7912-7927.
34. Hofflin F, Jack A, Riedel C, et al. Heterogeneity of the axon initial segment in interneurons and pyramidal cells of rodent visual cortex. *Front Cell Neurosci*. 2017;11:332.
35. Brackenbury WJ, Calhoun JD, Chen C, et al. Functional reciprocity between Na⁺ channel Na_v1.6 and β1 subunits in the co-ordinated regulation of excitability and neurite outgrowth. *Proc Natl Acad Sci U S A*. 2010;107:2283-2288.
36. Wengert ER, Wagley PK, Strohm SM, et al. Targeted Augmentation of Nuclear Gene Output (TANGO) of *Scn1a* rescues parvalbumin interneuron excitability and reduces seizures in a mouse model of Dravet syndrome. *Brain Res*. 2022; 1775:147743.
37. Ogiwara I, Iwasato T, Miyamoto H, et al. Nav1.1 haploinsufficiency in excitatory neurons ameliorates seizure-associated sudden death in a mouse model of Dravet syndrome. *Hum Mol Genet*. 2013;22:4784-4804.
38. Ogiwara I, Miyamoto H, Morita N, et al. Na_v1.1 localizes to axons of parvalbumin-positive inhibitory interneurons: A circuit basis for epileptic seizures in mice carrying an *Scn1a* gene mutation. *J Neurosci*. 2007;27:5903-5914.
39. Goff KM, Goldberg EM. Vasoactive intestinal peptide-expressing interneurons are impaired in a mouse model of Dravet syndrome. *Elife*. 2019;8:e46846.
40. Reddy DS, Thompson W, Calderara G. Molecular mechanisms of sex differences in epilepsy and seizure susceptibility in chemical, genetic and acquired epileptogenesis. *Neurosci Lett*. 2021; 750:135753.

41. Christian CA, Reddy DS, Maguire J, Forcelli PA. Sex differences in the epilepsies and associated comorbidities: Implications for use and development of pharmacotherapies. *Pharmacol Rev.* 2020;72:767-800.
42. Asadi-Pooya AA, Homayoun M. Sex differences in characteristics of idiopathic generalized epilepsies. *Neurol Sci.* 2021;42:2421-2424.
43. Liao P, Vajdic CM, Reppermund S, Cvejic RC, Srasuebkul P, Trollor JN. Mortality rate, risk factors, and causes of death in people with epilepsy and intellectual disability. *Seizure.* 2022;101:75-82.
44. Hesdorffer DC, Tomson T, Benn E, et al. Combined analysis of risk factors for SUDEP. *Epilepsia.* 2011;52:1150-1159.
45. Cetica V, Chiari S, Mei D, et al. Clinical and genetic factors predicting Dravet syndrome in infants with SCN1A mutations. *Neurology.* 2017;88:1037-1044.
46. Gerbatin RR, Augusto J, Boutouil H, Reschke CR, Henshall DC. Life-span characterization of epilepsy and comorbidities in Dravet syndrome mice carrying a targeted deletion of exon 1 of the Scn1a gene. *Exp Neurol.* 2022;354:114090.
47. Hawkins NA, Jurado M, Thaxton TT, et al. Soticlestat, a novel cholesterol 24-hydroxylase inhibitor, reduces seizures and premature death in Dravet syndrome mice. *Epilepsia.* 2021;62:2845-2857.
48. Williams AD, Kalume F, Westenbroek RE, Catterall WA. A more efficient conditional mouse model of Dravet syndrome: Implications for epigenetic selection and sex-dependent behaviors. *J Neurosci Methods.* 2019;325:108315.
49. O'Malley HA, Isom LL. Sodium channel β subunits: Emerging targets in channelopathies. *Annu Rev Physiol.* 2015;77:481-504.
50. Carvill GL, Mefford HC. Poison exons in neurodevelopment and disease. *Curr Opin Genet Dev.* 2020;65:98-102.
51. Oh Y, Waxman SG. Novel splice variants of the voltage-sensitive sodium channel alpha subunit. *Neuroreport.* 1998;9:1267-1272.
52. Mittal S, Tang I, Gleeson JG. Evaluating human mutation databases for "treatability" using patient-customized therapy. *Med.* 2022;3:740-759.
53. Gamache TR, Araki Y, Huganir RL. Twenty years of SynGAP research: From synapses to cognition. *J Neurosci.* 2020;40:1596-1605.
54. Yang R, Feng X, Arias-Cavieres A, et al. Upregulation of SYNGAP1 expression in mice and human neurons by redirecting alternative splicing. *Neuron.* 2023;111:1637-1650.e5.